British Journal of Pharmacology

British Journal of Pharmacology (2017) **174** 3623–3639 3623

RESEARCH PAPER

Antibiotic-induced dysbiosis of the microbiota impairs gut neuromuscular function in juvenile mice

Correspondence Maria Cecilia Giron, Department of Pharmaceutical and Pharmacological Sciences, Pharmacology Building, Gastrointestinal Pharmacology Unit, University of Padova, Largo Meneghetti, 2–35121 Padova, Italy. E-mail: cecilia.giron@unipd.it

Received 1 February 2017; **Revised** 18 July 2017; **Accepted** 19 July 2017

Valentina Caputi[1], Ilaria Marsilio[1], Viviana Filpa[2], Silvia Cerantola[1,3], Genny Orso[4], Michela Bistoletti[2], Nicola Paccagnella[1], Sara De Martin[1], Monica Montopoli[1], Stefano Dall'Acqua[1], Francesca Crema[5], Iole-Maria Di Gangi[6], Francesca Galuppini[7], Isabella Lante[3], Sara Bogialli[6], Massimo Rugge[7], Patrizia Debetto[1], Cristina Giaroni[2] and Maria Cecilia Giron[1]

[1]Department of Pharmaceutical and Pharmacological Sciences, University of Padova, Padova, Italy, [2]Department of Medicine and Surgery, University of Insubria, Varese, Italy, [3]San Camillo Hospital, Treviso, Italy, [4]IRCCS 'E. Medea' Bosisio Parini, Lecco, Italy, [5]Department of Internal Medicine and Therapeutics, Section of Pharmacology, University of Pavia, Pavia, Italy, [6]Department of Chemical Sciences, University of Padova, Padova, Italy, and [7]Department of Medicine, University of Padova, Padova, Italy

BACKGROUND AND PURPOSE

Gut microbiota is essential for the development of the gastrointestinal system, including the enteric nervous system (ENS). Perturbations of gut microbiota in early life have the potential to alter neurodevelopment leading to functional bowel disorders later in life. We examined the hypothesis that gut dysbiosis impairs the structural and functional integrity of the ENS, leading to gut dysmotility in juvenile mice.

EXPERIMENTAL APPROACH

To induce gut dysbiosis, broad-spectrum antibiotics were administered by gavage to juvenile (3weeks old) male C57Bl/6 mice for 14 days. Bile acid composition in the intestinal lumen was analysed by liquid chromatography-mass spectrometry. Changes in intestinal motility were evaluated by stool frequency, transit of a fluorescent-labelled marker and isometric muscle responses of ileal full-thickness preparations to receptor and non-receptor-mediated stimuli. Alterations in ENS integrity were assessed by immunohistochemistry and Western blot analysis.

KEY RESULTS

Antibiotic treatment altered gastrointestinal transit, luminal bile acid metabolism and bowel architecture. Gut dysbiosis resulted in distorted glial network, loss of myenteric plexus neurons, altered cholinergic, tachykininergic and nitrergic neurotransmission associated with reduced number of nNOS neurons and different ileal distribution of the toll-like receptor TLR2. Functional defects were partly reversed by activation of TLR2 signalling.

CONCLUSIONS AND IMPLICATIONS

Gut dysbiosis caused complex morpho-functional neuromuscular rearrangements, characterized by structural defects of the ENS and increased tachykininergic neurotransmission. Altogether, our findings support the beneficial role of enteric microbiota for ENS homeostasis instrumental in ensuring proper gut neuromuscular function during critical stages of development.

Abbreviations

CA, cholic acid; ChAT, choline acetylase; EGCs, enteric glial cells; ENS, enteric nervous system; GFAP, glial fibrillary acidic protein; nNOS, neuronal NOS; SP, substance P; TCA, taurocholic acid; TLRs, toll-like receptors

DOI:10.1111/bph.13965

Introduction

The naturally occurring commensal microbiota consists of about 10^{14} bacterial cells belonging to approximately 500–1000 species that symbiotically colonize the human gut (Foster and McVey Neufeld, 2013). The individual composition of the microbiota is constantly altered by several factors including, but not limited to, genetics, age, sex, diet, medicines and lifestyle. In general, the interactions between commensal microbiota and its host are beneficial. The intestinal microbiota is an indispensable organ for the homeostasis of the host, participating in nutrient processing and production of essential compounds, such as short-chain fatty acids and some vitamins, and contributing to the maturation of the gastrointestinal (GI) system and shaping the immune system. Interestingly, the total metabolic capacity of the commensal microbiota is comparable to the metabolic capacity of the liver (Foster and McVey Neufeld, 2013; Sommer and Bäckhed, 2013).

Several studies carried out in animal models have underlined the bottom-up effects of the enteric microbiota on the development and maturation of the enteric nervous system (ENS) (Hyland and Cryan, 2016). In normal conditions, the intestinal epithelial barrier and mucous layer separate the ENS, which comprises two distinct interconnected networks of neuronal and glial cells innervating all the GI tract - the submucosal and myenteric plexuses - from the microbiota (Furness, 2012; Coelho-Aguiar *et al.*, 2015). However, enteric neurons and glial cells can sense microbes through pattern recognition receptors, such as the **toll-like receptors**, TLRs) (Anitha *et al.*, 2012; Brun *et al.*, 2013) and other neurochemical receptors as well as through microbial-derived components, microvescicles, neuroactive metabolites or mucosal elements (e.g. enteroendocrine-cell derived mediators) (Hyland and Cryan, 2016). Recently, the effects of gut microbiota-mediated signalling on ENS function has been investigated in many different animal models, from animals fed with specific dietary treatments to transgenic animals or germ-free rodents. Most of these studies showed that perturbations of microbial communities may affect postnatal ENS development, inducing adaptive changes in both enteric neurons and glia (Kabouridis *et al.*, 2015). Such microbiota-induced ENS plasticity may not only influence GI functions (Kabouridis and Pachnis, 2015) but can also potentially lead to CNS responses, *via* gut-to-brain signalling (Borre *et al.*, 2014).

Indeed, the hypothesis that alterations in gut microbiota may lead to the onset of acute or chronic diseases, both in the gut and in the brain, has been proposed by several groups (Foster and McVey Neufeld, 2013; Kabouridis and Pachnis, 2015; Hyland and Cryan, 2016). Specifically, several studies have shown that changes in microbiota composition may be related to functional or psychiatric disorders such as irritable bowel syndrome (IBS) (Kennedy *et al.*, 2014), autism and cognitive impairment (Mayer *et al.*, 2014; Fröhlich *et al.*, 2016). These findings support the existence of a local mutual interaction between the enteric microbiota and the ENS, but also an indirect influence of CNS function, *via* activation of neuroendocrine and metabolic pathways, suggesting that the relative abundance and diversity of the various microbe constituents is essential for the development and maturation of host CNS and ENS.

In particular, the incidence of paediatric IBD is increasing worldwide with a dramatic rise of Crohn's disease, involving especially those children previously exposed to antibiotic courses (Ungaro *et al.*, 2014). Because adolescence and early adulthood are critical times for the development and maturation of the nervous system and because the ileum represents the intestinal segment mostly affected by Crohn's disease, we have, here, investigated the effects of gut dysbiosis induced by antibiotics on the morphology and function of the ENS in juvenile mice.

Methods

Animals

All animal care and experimental procedures were approved by the Animal Care and Use Ethics Committee of the University of Padova and by the Italian Ministry of Health (authorization number: 1142/2015-PR) and were performed in accordance with national and EU guidelines for the handling and use of experimental animals. Animal studies are reported in compliance with the ARRIVE guidelines (Kilkenny *et al.*, 2010; McGrath and Lilley, 2015).

Juvenile male C57BL/6 J mice (3 ± 1 weeks old, body weight 18 ± 1 g, Charles River Laboratories, Italy) were housed in individually ventilated cages (four animals per cage) at the conventional animal facility of the Department of Pharmaceutical and Pharmacological Sciences of the University of Padova, under controlled environmental conditions (temperature 21 ± 1°C; relative humidity 60–70%) with free access to standard laboratory chow and tap water and maintained at a regular 12/12 h light/dark cycle.

Treatments

To induce gut dysbiosis in mice, we used a previously established pharmacological model, which reproduces a germ-free-like phenotype (Reikvam *et al.*, 2011; Josefsdottir *et al.*, 2017). Briefly, a cocktail of broad spectrum antibiotics (50 $mg \cdot kg^{-1}$ vancomycin, 100 $mg \cdot kg^{-1}$ **neomycin**, 100 $mg \cdot kg^{-1}$ metronidazole and 100 $mg \cdot kg^{-1}$ ampicillin) was administered to mice every 12 h for 14 days by oral gavage (100 μL per mouse), using a stainless steel feeding tube without prior sedation of the animals (Reikvam *et al.*, 2011; Brun *et al.*, 2013); this constituted the ABX-treated group. Control (CNTR) mice were treated similarly with vehicle (tap water). Animals were randomized to treatment groups. To normalize gut microbiota, mouse colonies from both groups were housed in the same room and generally in the same cages and maintained by the same personnel. In a sub-group pf mice, the TLR2 agonist Pam3CysSerLys4 (**Pam3CSK4**; Invivogen, San Diego, USA), was administered (i.p.; 2 $mg \cdot kg^{-1}$ in 0.9% saline) to ABX-treated mice for seven consecutive days during the second week of antibiotic treatment. At the end of procedures, animals were killed by cervical dislocation. All the following analytical procedures were conducted blindly.

Bile acids extraction and HPLC-MS analysis

The concentration of the bile acids, **cholic acid** (CA) and **taurocholic acid** (TCA) in the small intestinal lumen was evaluated by LC quadrupole time-of-flight MS (LC-QTOF-MS). Stool samples (50 mg) were collected 12 h after the last antibiotic treatment from the small intestinal lumen, homogenized and extracted with 1 mL acetonitrile and then centrifuged for 10 min at 12 000 × *g*. Supernatants were diluted 1:10 with a mobile phase (water and acetonitrile, 50:50 v/v, acidified with 5 mM ammonium acetate). Randomized samples were analysed by LC-QTOF-MS with a Ultra-high performance liquid chromatography (UHPLC) system (Agilent Series 1200; Agilent Technologies, Palo Alto, CA, USA), consisting of vacuum degasser, auto-sampler, a binary pump and a column oven coupled to QTOF-MS mass analyser (Agilent Series 6520; Agilent Technologies). The eluent flow rate was 0.25 mL·min^{-1} through the analytical column Kinetex C-18 (2.6 μm, 100 × 2.1 mm i.d., Phenomenex, Italy) thermostated at 18°C. The mobile phase gradient profile was as follows (t in min): t0, B = 0%; t4, B = 100%; t6, B = 100%; t7, B = 0%; t14, B = 0%. The QTOF system was equipped with an ESI, operating in dual ESI mode and negative acquisition (capillary voltage, 3500 V; nebulizer pressure, 30 ψ; drying gas, 10 L·min^{-1}; gas temperature, 350°C; fragmentor voltage, 170 V; skimmer 65 V). Centroid full scan mass spectra were recorded over the range 50–2000 m/z with a scan rate of 1 spectra·s^{-1}. Tandem MS fragmentation of each pseudomolecular ion $[M\text{-}H]^-$ was performed in target MS mode, setting at least 20 scans at scan rate of two scan·s^{-1} with a peak width of 4 amu and retention time tolerance of 1 min. Standard solutions of TCA and CA (0.5 μg·mL^{-1}) were used in flow injection analysis for the optimization of the fragmentor voltage and collision energies (Table 1). A QTOF calibration was daily performed with the manufacturer's solution. For all chromatographic runs, the ionic signal at *m/z* 112.9856 referable to formic acid was set as lock mass. Mass spectra acquisition and data analysis were performed with Masshunter Workstation B.07.00 software (Agilent Technologies). All analyses performed showed a mass accuracy better than 5 ppm, allowing the correct identification of the target bile acids. Quantitation was achieved by plotting the analyte area, corresponding to the extracted ion chromatogram with a window span of 20 ppm of the $[M\text{-}H]^-$. To avoid inaccuracies due to matrix effects, the standard addition method with least squares regression was carried out, by adding to each sample the standard analytes in duplicate at three concentration levels within the range of 50–4000 μg·g^{-1} for TCA and 750–6000 μg·g^{-1} for CA. Limits of detection corresponding to an S/N of 3 were assessed from diluting the lowest quantified concentration of the real samples (Table 1).

Macroscopic and histological assessment

Mice were killed by cervical dislocation, and the whole intestine (from stomach to anus) was excised. The entire length of the stomach, small intestine and caecum was measured. The weight of caecum with its contents was also measured. Ileum, caecum and stomach specimens, after being fixed in 10% buffered formalin, were embedded in paraffin and cut into 4 μm sections. Tissue sections were then stained with haematoxylin and eosin (H&E). Smooth muscle thickness and lumen diameter of the stomach, ileum and caecum were analysed in 10 H&E sections for each group (Dall'Olmo *et al.*, 2014).

Gastrointestinal transit

The GI transit was assessed by evaluating the distribution through the bowel of orally gavaged FITC-labelled dextran (FITC-dextran, 70 kDa; 25 mg·mL^{-1} in 0.9% saline solution). After 30 min, mice were randomly and killed, and the GI tract from stomach to distal colon was collected and placed into Krebs solution. The stomach and caecum were analysed separately while the small intestine and the colon were divided into 10 and 3 segments of equal length respectively. Luminal contents from each segment were collected and cleared by centrifugation (10 000 × *g* for 10 min at 4°C). FITC-dextran intensity of each segment was measured fluorimetrically at 492/521 nm (Victor, PerkinElmer; Wallac Instruments, Turku, Finland). The transit of FITC-dextran along the GI tract was determined by calculating the percentage fluorescence for each segment and the geometric centre (GC) for the distribution of the fluorescent probe using the following equation: GC = Σ (% of total fluorescent signal per segment × segment number)/100 (Brun *et al.*, 2013).

Pellet frequency and faecal water content

Faecal pellet output was examined daily at a fixed time in CNTR and ABX mice as previously described (Li *et al.*, 2006). Randomized mice were individually placed in a novel environment (clean cage) and observed for 60 min. The number of pellets per mouse was recorded and weighed (wet weight). Pellets were subsequently dried overnight at 65°C and reweighed until achieving a constant weight (dry weight). Water content was calculated as the difference between the wet weight and dry weight (McQuade *et al.*, 2016).

In vitro contractility studies

Contractility studies were performed as previously described (Giron *et al.*, 2008; Brun *et al.*, 2013; Zoppellaro *et al.*, 2013). Segments (1 cm in length) of mouse distal ileum, proximal to the ileocaecal junction, were isolated and mounted along the longitudinal axis in organ baths containing 10 mL of

Table 1

Experimental conditions for the LC/MS acquisition of selected bile acids

Bile acid	Retention time (min)	Theoretical pseudomolecular ions, $[M\text{-}H]^-$, m/z	Collision energy (eV)	LOD, (μg·g^{-1})
TCA	8.03	514.2844	50	7
CA	8.50	407.2803	35	3

LOD; Limit of detection.

oxygenated (95% O_2 and 5% CO_2) and heated (37°C) Krebs solution (in mM: NaCl 118, $NaHCO_3$ 25, $C_6H_{12}O_6$ 11, KCl 4.7, $CaCl_2$ $2H_2O$ 2.5, $MgSO_4$ 1.2, K_2HPO_4 1.2). Changes in mechanical activity of the ileal segments were recorded by isometric transducers (World Precision Instruments, Berlin, Germany) connected to a quad bridge amplifier and PowerLab 4/30 data acquisition system using LabChart6 software (ADInstruments, Besozzo, VA, Italy).

After 45 min equilibration, ileal segments were stretched passively to an initial tension of 0.5 g and brought to their optimal point of length-tension relationship using 1 μM **carbachol** (Brun *et al.,* 2013; Zoppellaro *et al.,* 2013). Ileal segments were treated with carbachol to study cholinergic effects or with 60 mM KCl solution to elicit depolarization-induced contraction. After the equilibration period, concentration–effect curves to carbachol (0.001–100 μM) were obtained cumulatively and plotted into a nonlinear regression model (fitted to a sigmoidal equation) to calculate EC_{50} and maximal tension (Emax) values. Neuronally mediated contractions were obtained through electrical field stimulation (EFS, 0–40 Hz; 1 ms pulse duration; 10 s pulse-trains, 40 V) using platinum electrodes connected to an S88 stimulator (Grass Instrument, Quincy, MA, USA). In order to establish NANC nerve stimulation, both **guanethidine** (1 μM) and **atropine** (1 μM) were added to Krebs solution and ileal tissues were allowed to equilibrate for 1 h prior to EFS stimulation. Under NANC conditions, the effects of the non-selective NOS inhibitor **L-NAME**, 100 μM; preincubation time = 20 min) or the **inducible NOS** (iNOS) inhibitor **1400 W** (10 μM; preincubation time = 20 min) were recorded on 10 Hz-EFS-induced on-relaxations. In order to evaluate the influence of tachykininergic neurotransmission on ileal contraction, the 10 Hz EFS-mediated tachykininergic off-response was assessed in presence of 100 μM L-NAME and 10 μM **L732138** (**NK_1 receptor** antagonist) under NANC conditions. Contractile responses were expressed as g tension·per g dry tissue weight of ileal segments.

Under NANC conditions, EFS induced a primary on-relaxation of ileal full thickness segments that was calculated as AUC and normalized per g dry tissue weight to allow comparisons between tissue samples. However, it should be considered that the obtained quotient having the dimension 'minutes' does not have the significance of an average duration, as previously described (Currò *et al.,* 2002). The effect of ABX-induced changes and/or *in vitro* pharmacological treatment on EFS-induced inhibitory responses was expressed as percentage relaxations with respect to values obtained in CNTR preparations (Zizzo *et al.,* 2003).

Histochemical analysis of acetylcholinesterase (AChE) and immunohistochemical analysis of choline acetylase (ChAT) in ileal whole-mount preparations

Distal ileum 10 cm segments were filled with fixative solution (4% paraformaldehyde in PBS) for 1 h at room temperature. Using a dissecting microscope, whole-mount preparations consisting of the longitudinal muscle with the myenteric plexus attached (LMMPs) were prepared as previously described (Brun *et al.,* 2013). For **AChE** staining, ileum LMMPs were incubated in fresh copper buffer solution (containing per 100 mL distilled H_2O; 885 mg sodium acetate trihydrate, 115.6 mg acetylthiocholine iodide, 75 mg glycine, 50 mg $CuSO_45H_2O$, 7.2 mg ethopropazine, pH 5.6) for 2 h followed by two washes in distilled H_2O. After incubation in 1.25% (w/v) Na_2S $9H_2O$ for 1 min, tissues were washed in distilled H_2O and mounted on a glass slide using a Mowiol Mounting Medium [100 mM Tris–HCl (pH 8.5), 9% Mowiol 4–88, 25% glycerol and 0.1% DABCO] and observed using a Leica DM4000 B microscope (Leica Microsystems GmbH, Wetzlar, Germany). $AChE^+$ myenteric neurons were counted per myenteric ganglia area.

For **ChAT** immunohistochemistry, LMMPs from CNTR and ABX mice were washed in PBT (PBS with 0.2% Triton X-100) for 45 min with gentle shaking. After blocking non-specific sites with PBT containing 2% BSA for 1 hour at room temperature, LMMPs were incubated with ChAT primary antibody (Supporting Information Table S1) diluted in PBT/BSA 2% overnight at room temperature. The following day, LMMPs were washed for 45 minutes in PBT and incubated with secondary antibody (Supporting Information Table S1) for 2 hours at room temperature. After three subsequent 15-minutes washes with PBT, LMMPs were mounted on glass slides using a Mowiol Mounting Medium. Images were acquired using a Nikon D-Eclipse C1 confocal microscope (Nikon Instruments, Florence, Italy) equipped with an oil-immersion Nikon Plan-Apo 60×/1.4 objective (see below). Images were captured at identical acquisition exposure-time conditions and thresholded to allow ImageJ software (version 1.48a) to select and measure only ChAT stained segments. In ileal LMMPs, changes in the immunoreactivity for ChAT were assessed by analysing the density index of labelling per myenteric ganglia area (6 animals per group, 20 fields per preparation at 60× magnification).

Immunohistochemistry on ileal whole-mount preparations

LMMPs from CNTR and ABX mice were gently stretched and pinned down on a wax support as previously described (Brun *et al.,* 2013) and washed in PBT (PBS with 0.2% Triton X-100) for 45 min with gentle shaking. For **substance P** (SP) immunostaining, the excised tissue was initially incubated for 4 h in Krebs solution, bubbled with 95% O_2 and 5% CO_2 containing colchicine (0.1 $g{\cdot}L^{-1}$) in order to enhance the immunofluorescence of SP^+ neurons (Messenger and Furness, 1990). After blocking non-specific sites with PBT containing 2% BSA for 1 h at room temperature, LMMPs were incubated with primary antibodies (Supporting Information Table S1) diluted in PBT/BSA 2% overnight at room temperature. The following day, LMMPs were washed for 45 min in PBT and incubated with secondary antibodies (Supporting Information Table S1) for 2 h at room temperature. After three subsequent 15 min washes with PBT, LMMPs were mounted on glass slides using a Mowiol Mounting Medium. Negative controls were obtained by incubating sections with isotype-matched control antibodies at the same concentration as primary antibody and/or pre-incubating each antibody with the corresponding control peptide (final concentration as indicated by manufacturer's instructions).

Immunohistochemistry on ileal frozen sections

Immunofluorescence was performed on distal ileum frozen tissues (0.5 cm segments) embedded in optimal cutting temperature (OCT) Mounting Medium and sectioned (7 μm-thick) with a cryostat-microtome (Leica CM 1850 UV, Milan, Italy). The sections were mounted onto Superfrost Plus slides and analysed by immunohistochemistry as previously described (Zoppellaro *et al.,* 2013; Antonioli *et al.,* 2014a; Antonioli *et al.,* 2014b). Briefly, ileal sections from CNTR and ABX mice were fixed for 15 min with 4% paraformaldehyde in PBS, washed in Tris-buffer saline (TBS) and incubated with 0.05 M NH_4Cl. Ileum samples were permeabilized and blocked with a solution of TBS containing 2% BSA and 0.3% Triton X-100 for 1 h. Then, ileal frozen sections were incubated with the primary antibodies (Supporting Information Table S1) optimally diluted in TBS with 0.5% BSA for 2 h at room temperature. Immunocomplexes were visualized by incubating samples with the corresponding secondary antibodies (Supporting Information Table S1) for 1 h at room temperature. Nuclei were stained with TOTO-3 iodide (1:500, Thermo Fisher Scientific, Milan Italy), added together with the secondary antibodies. Negative controls were obtained as described in the previous section titled immunohistochemistry on ileal whole-mount preparations.

Acquisition and analysis of images

Images were acquired using a Nikon D-Eclipse C1 confocal microscope (Nikon Instruments, Florence, Italy) equipped with an oil-immersion Nikon Plan-Apo 60×/1.4 objective or a low-magnification Nikon Plan Fluor 20×/0.5 objective. Fluorophores were visualized using a 488 nm excitation filter and 515/530 nm emission filter for Alexa Fluor 488, 543 nm excitation filter and 590/650 nm emission filter for Alexa Fluor 555 or Dy Light 549 and 637 nm excitation and 650 LP (long pass) nm emission filter for TOTO-3 iodide. Z-series images (15 planes) of 1024 × 1024 pixels were captured and processed as maximum intensity projections. All microscope settings were set to collect images below saturation and were kept constant for all images.

In ileal myenteric plexus, total neuron population analysis was performed on LMMP preparations, obtained from six animals per group, by counting HuC/D^+ myenteric cells, and the distribution of nitrergic and tachykininergic neurons was evaluated by counting HuC/D^+/neuronal NOS (**nNOS**)$^+$ and $HuC/D^+/SP^+$ neuronal cells respectively. Areas of myenteric ganglia, digitized by capturing 20 fields per preparation at 20× magnification, were measured by tracing boundaries around stained cell somas (HuC/D). The number of HuC/D^+ or $HuC/D^+/nNOS^+$ or $HuC/D^+/SP^+$ neurons was counted per myenteric ganglia area, as previously described (Stenkamp-Strahm *et al.,* 2013; Robinson *et al.,* 2016). In ileal LMMP whole-mount preparations changes in the immunoreactivity for S100β, ChAT and TLR2 were assessed by analysing the density index of labelling per myenteric ganglia area (six animals per group, 20 fields per preparation at 60× magnification). Images were captured at identical acquisition exposure-time conditions and thresholded to allow ImageJ software (version 1.48a) to select and measure only stained segments. In ileal cryosections, changes in SP and TLR2 immunoreactivity were evaluated by calculating the density index of labelling per tissue area, as previously described (Stenkamp-Strahm *et al.,* 2013).

Western immunoblot analysis

Total proteins from mouse ileal samples were extracted in RIPA buffer (150 mM NaCl, 50 mM Tris–HCl, 0.25% wt·vol^{-1} sodium deoxycholate, 0.1% Nonidet P-40, 100 μM $NaVO_4$, 1 mM NaF, 1 mM phenylmethylsulfonyl fluoride, 10 μg·mL^{-1} aprotinin, 10 μg·mL^{-1} leupeptin). Particulate material was removed by centrifugation. Proteins were separated by SDS PAGE and then transferred to nitrocellulose membrane. Membranes were then blocked for 1 h with 5% non-fat dried milk in PBS at room temperature and probed with the following primary antibodies: rabbit polyclonal anti-mouse nNOS (1:500; Thermo Fisher Scientific, Milan, Italy) and mouse monoclonal anti-human β actin (1:10 000) over night at 4°C. After repeated washings with 0.1% Tween-20 in TBS, membranes were incubated with the proper secondary antibodies, conjugated with horseradish peroxidase. The immunoreactive bands were visualized using enhanced chemiluminescence (ECL, Millipore, Milano, Italy) (Brun *et al.,* 2013). Experiments were performed at least four times for each different preparation. Signal intensity of immunoreactive bands was analysed by the Quantity One software (Bio-Rad Laboratories Srl) and expressed as intensity * mm^2 (INT * mm^2).

Data and statistical analysis

The data and statistical analysis in this study comply with the recommendations on experimental design and analysis in pharmacology (Curtis *et al.,* 2015). All the experiments were analysed by investigators blinded to the treatments. All data are expressed as mean ± SEM, except for the GC, which was presented as median, interquartile range and minimum–maximum. Statistical significance was calculated with the paired or unpaired Student's *t*-test for two-sample comparisons, one-way ANOVA followed by Newman–Keuls *post hoc* test for multiple comparison, two-way ANOVA followed by Bonferroni's multiple comparison test for *post hoc* analysis or the non-parametric Mann–Whitney's *U*-test for independent variables using GraphPad Prism 3.03 (San Diego, CA, USA). The differences between groups were considered significant when $P < 0.05$; 'N' values indicate the number of animals. *Post hoc* tests were run only if F achieved $P < 0.05$ and there was no significant variance inhomogeneity.

Materials

Unless otherwise specified, all chemicals were obtained from Sigma Aldrich (Milan, Italy) and were of the highest available analytical grade. OCT was purchased from Kaltek (Padua, Italy), PFA was from Electron Microscopy Sciences-Società Italiana Chimici (Rome, Italy), Triton-X-100 was from Applichem (Milan, Italy), TRIzol was from Invitrogen (Milan, Italy) and DNase Free was from Ambion (Milan, Italy).

Nomenclature of targets and ligands

Key protein targets and ligands in this article are hyperlinked to corresponding entries in http://www.guidetopharmacology.org, the common portal for data from the IUPHAR/BPS Guide to PHARMACOLOGY (Southan *et al.,* 2016), and are permanently archived in the Concise Guide to PHARMACOLOGY 2015/16 (Alexander *et al.,* 2015a,b,c).

Results

Antibiotic exposure induces a germ-free-like phenotype

Mice orally treated with the antibiotic cocktail for 14 days (ABX-treated mice) showed no differences in the percentage of weight gain (+8.9 ± 1.3%) compared to control (CNTR) mice (+8.4 ± 1.2%, *N* = 20 mice per group). ABX-treated mice displayed a significant increase in caecum weight (*N* = 5 mice per group; Supporting Information Figure S1A, B), associated with a significant reduction of spleen weight (*N* = 5 mice per group; Supporting Information Figure S1C). Histological analysis of intestinal sections showed a significant increase of the thickness of the *muscularis externa* in the stomach, ileum and caecum of ABX mice compared to CNTR animals. However, the antibiotic treatment affected only the caecum diameter and length, not those of the gastric and ileal lumen (Table 2). These findings are in agreement with other reports showing the occurrence of macroscopic changes in the intestine of germ-free or antibiotic-treated mice (Reikvam *et al.*, 2011; Grasa *et al.*, 2015; Ge *et al.*, 2017).

Gastrointestinal motility is impaired in antibiotic-treated mice

Studies in germ-free animals have shown impaired intestinal transit and motor function (Barbara *et al.*, 2005). In juvenile mice, antibiotic-induced microbiota dysbiosis induced a significant decrease of GI transit, as shown by the higher content of the non-absorbable FITC-labelled dextran in the upper part of the GI tract (Figure 1A). Accordingly, ABX-treated mice displayed a significant reduction of the GC compared with that of CNTR mice (*N* = 10 mice per group; Figure 1B) and delayed gastric emptying, as shown by a 4.5-fold increase in the gastric fluorescent probe levels (*N* = 10 mice per group; Figure 1C). The delay of GI transit in ABX-treated mice was paralleled by a significant reduction in stool expulsion frequency (*N* = 15 mice per group; Supporting Information Figure S2A), evaluated during 1 h collection period, and by a decrease of both dry and wet pellet weights and by an increase of faecal water content (*N* = 15 mice per group; Supporting Information Figure S2B,C), suggesting the presence of constipation and altered intestinal water secretion. In agreement with other studies (Kuribayashi *et al.*, 2012), the analysis of the profile of bile acids in the small intestine faecal content of ABX-treated mice revealed around 3.5-fold increase in TCA, whereas CA decreased to below detectable levels (*N* = 5 mice per group; Figure 1D), suggesting that the production of CA, following the deconjugation of TCA by enterobacteria, was strongly impaired by antibiotic-induced microbiota dysbiosis.

Antibiotic-induced microbiota dysbiosis causes morphological abnormalities in the architecture of the myenteric plexus of juvenile mice

Development of the intestinal microbiota is a key dynamic process in the first years of life, a critical stage for ENS development and maturation (Brun *et al.*, 2013; Borre *et al.*, 2014). Changes in microbiota composition and/or signalling are known to influence ENS morphology (Brun *et al.*, 2013; Hyland and Cryan, 2016). In the myenteric plexus of ABX-treated mouse ileum, the numbers of HuC/D-stained neurons were significantly lower than in CNTR mice (*N* = 6 mice per group,; Figure 2A, B). In addition, antibiotic treatment induced distortion of enteric glial cell (EGC) processes within myenteric ganglia, as shown by glial fibrillary acidic protein $(GFAP)^+$ labelling, and a marked increase of S100β density index (by 1.4-fold, compared with CNTR, *N* = 6 mice per group; Figure 2C–E).

Antibiotic-induced microbiota dysbiosis alters excitatory neuromuscular contractility

As longitudinal muscle contractile activity underlies the preparative phase of the peristaltic reflex and is synchronous with circular muscle contraction during peristalsis, changes in its efficiency may influence the whole propulsive bowel activity (Smith and Robertson, 1998). The effects of antibiotic treatment on neuromuscular function were thus examined *in vitro* by measuring tension changes in isolated ileal preparations. Ileal segments of ABX-treated mice displayed spontaneous contractile activity consisting of phasic contractions with an amplitude of 210 ± 12.3 mg and a frequency of 32.6 ± 0.2 cpm, with no differences from those in CNTR mice (amplitude = 234 ± 13.2 mg and frequency = 32.4 ± 0.3 cpm, *N* = 20 mice per group). To evaluate changes in the excitatory neuromuscular response following antibiotic treatment, cumulative concentration–response curves to the non-selective cholinergic agonist, carbachol were performed. Ileal segments from ABX-treated mice showed a significant

Table 2

Histological and morphological assessment of mouse stomach, small intestine and caecum following treatment with vehicle (CNTR) or antibiotics (ABX)

Histological and morphological parameters	Stomach		Small intestine		Caecum	
	CTRL (*N* = 5)	ABX (*N* = 5)	CTRL (*N* = 5)	ABX (*N* = 5)	CTRL (*N* = 5)	ABX (*N* = 5)
Muscularis externa thickness (mm)[a]	0.056 ± 0.003	0.170 ± 0.015*	0.056 ± 0.003	0.076 ± 0.003[a]	0.100 ± 0.005	0.143 ± 0.008*
Lumen diameter (mm)[a]	8.33 ± 0.35	8.67 ± 0.32	2.60 ± 0.55	3.03 ± 0.98	4.20 ± 0.15	9.17 ± 0.12*
Organ length (cm)	1.37 ± 0.07	1.41 ± 0.04	29.50 ± 1.32	32.73 ± 0.94	3.03 ± 0.08	4.43 ± 0.14*

[a]measured in distal ileum. Statistical Data shown are means+ SEM; N = number of animals

*$P < 0.05$, significantly different from CNTRL; unpaired Student's t-test.

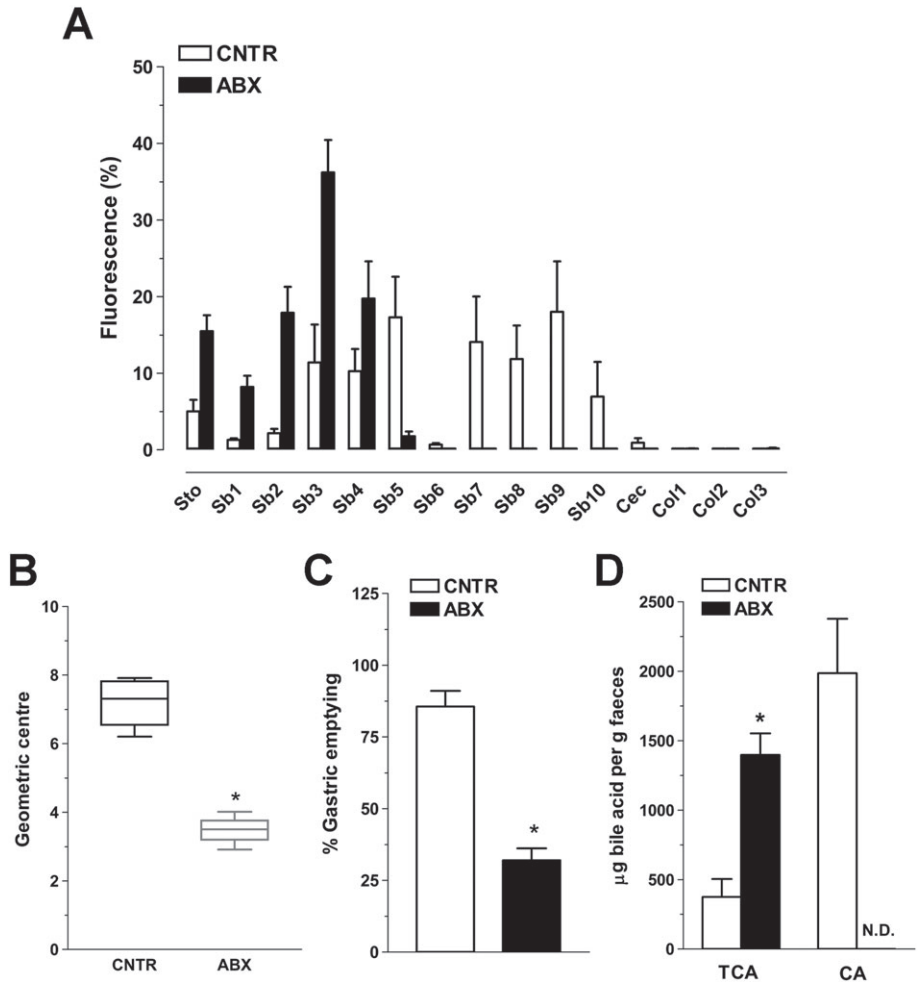

Figure 1

Antibiotic-induced microbiota dysbiosis affects GI transit and bile acid metabolism. (A) Percentage of non-absorbable FITC-labelled dextran distribution throughout the GI tract consisting of stomach (Sto), small bowel (Sb 1–10), caecum (Cec) and colon (Col 1–3); (B) geometric centre (GC) of non-absorbable FITC-dextran; (C) percentage of gastric emptying in CNTR and ABX-treated mice (N = 10 mice per group). (D) Changes in the levels of TCA and CA in the ileal lumen of CNTR and ABX-treated mice (N = 5 mice per group). N.D. indicates levels below the limit of detection ($<3\mu g \cdot g^{-1}$ for CA). Data are reported as mean ± SEM for panels (A), (C) and (D) and as median, minimum, maximum, upper and lower quartiles for panel (B). *$P < 0.05$, significantly different from CNTR; non-parametric Mann–Whitney's U-test (panel B) or unpaired Student's t-test (panels C and D).

downward shift of the concentration–response curve to carbachol and a consequent decrease in maximum response, Emax falling to about 50% of the CNTR value (N = 8 mice per group; Figure 3A). Ileal muscular response to the depolarizing agent KCl (60 mM) was also significantly decreased in ABX-treated mice (N = 8 mice per group; Figure 3B). To confirm that ileal contraction changes in ABX-treated mice were caused by alterations in neuromuscular function, we evaluated the effect of EFS at increasing frequencies of stimulation on ileal preparations. In ABX-treated mouse ileum, the EFS-elicited contractions significantly decreased, by about 60% of the CNTR value at 10 Hz (N = 8 mice per group; Figure 3C), confirming development of alterations in the excitatory neurotransmission. We previously demonstrated that in mouse ileum, EFS-mediated responses to frequencies up to 10 Hz are of neuronal cholinergic origin, being sensitive to both **tetrodotoxin** and atropine (Brun *et al.*, 2013). In ileal whole-mount preparations of ABX-treated mice, the number of $AChE^+$ myenteric neurons and ChAT immunoreactivity was significantly reduced compared with CNTR mice (N = 6 mice per group; Figure 3D–G), suggesting that the cholinergic neuronal network is significantly affected by microbiota dysbiosis.

Antibiotic-induced microbiota dysbiosis affects inhibitory neurotransmission

Subsequently, we evaluated the effect of microbiota dysbiosis on the enteric nitrergic transmission, which represents the main inhibitory neurotransmission on the intestinal neuromuscular function (Filpa *et al.*, 2017). **NO**-mediated relaxation responses of mouse ileum to transmural stimulation

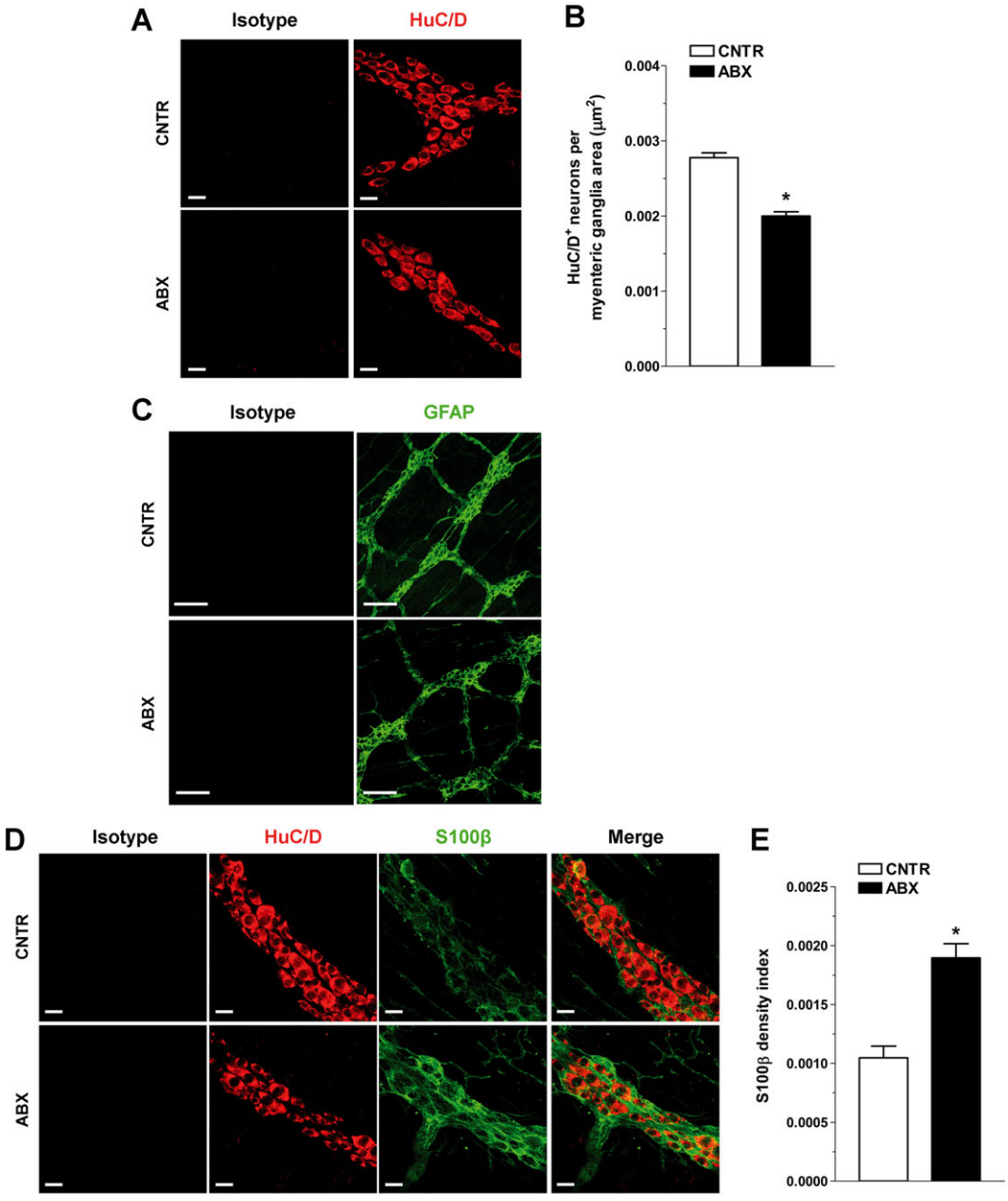

Figure 2

Effects of antibiotic treatment on myenteric plexus architecture. (A) Representative confocal microphotographs showing the distribution of HuC/D (red, pan-neuronal marker) and (B) number of HuC/D$^+$ neurons per myenteric ganglia area in LMMP preparations from CNTR and ABX-treated mice (N = 6 mice per group). Scale bars = 22 μm. (C and D) Representative confocal photomicrographs showing the distribution of GFAP (green), S100β and HuC/D (green and red, respectively) in LMMP preparations from CNTR and ABX-treated mice (N = 6 mice per group). Scale bars = 100 μm (C) and 22 μm (D). (E) S100β density index in LMMP preparations of CNTR and ABX-treated mice (N = 6 mice per group). Data are reported as mean ± SEM. *$P < 0.05$ significantly different from CNTR; unpaired Student's t-test (panels B and E).

were evaluated in the presence of guanethidine and atropine, and the NO dependence of the relaxation was confirmed by incubation with the non-selective NOS inhibitor L-NAME prior to EFS (Zizzo *et al.*, 2004). NANC-evoked on-relaxations at 10 Hz stimulation frequency markedly increased in ABX-treated mice, compared with CNTR (by 70%, N = 8 mice per group; Figure 4A, B). In ABX mice, pretreatment with 1400 W, a selective inhibitor of iNOS, did not affect 10 Hz EFS-induced on-relaxations in NANC conditions (Figure 4B) whereas addition of L-NAME abolished the on-relaxation response induced by EFS in CNTR mice, but not in ABX-treated mice (N = 8 mice per group; Figure 4B), suggesting enhancement of other inhibitory neurotransmitter pathways, after microbiota dysbiosis (Zizzo *et al.*, 2003). To further investigate the effect of dysbiosis on the enteric nitrergic neurotransmission, we evaluated the distribution of nitrergic

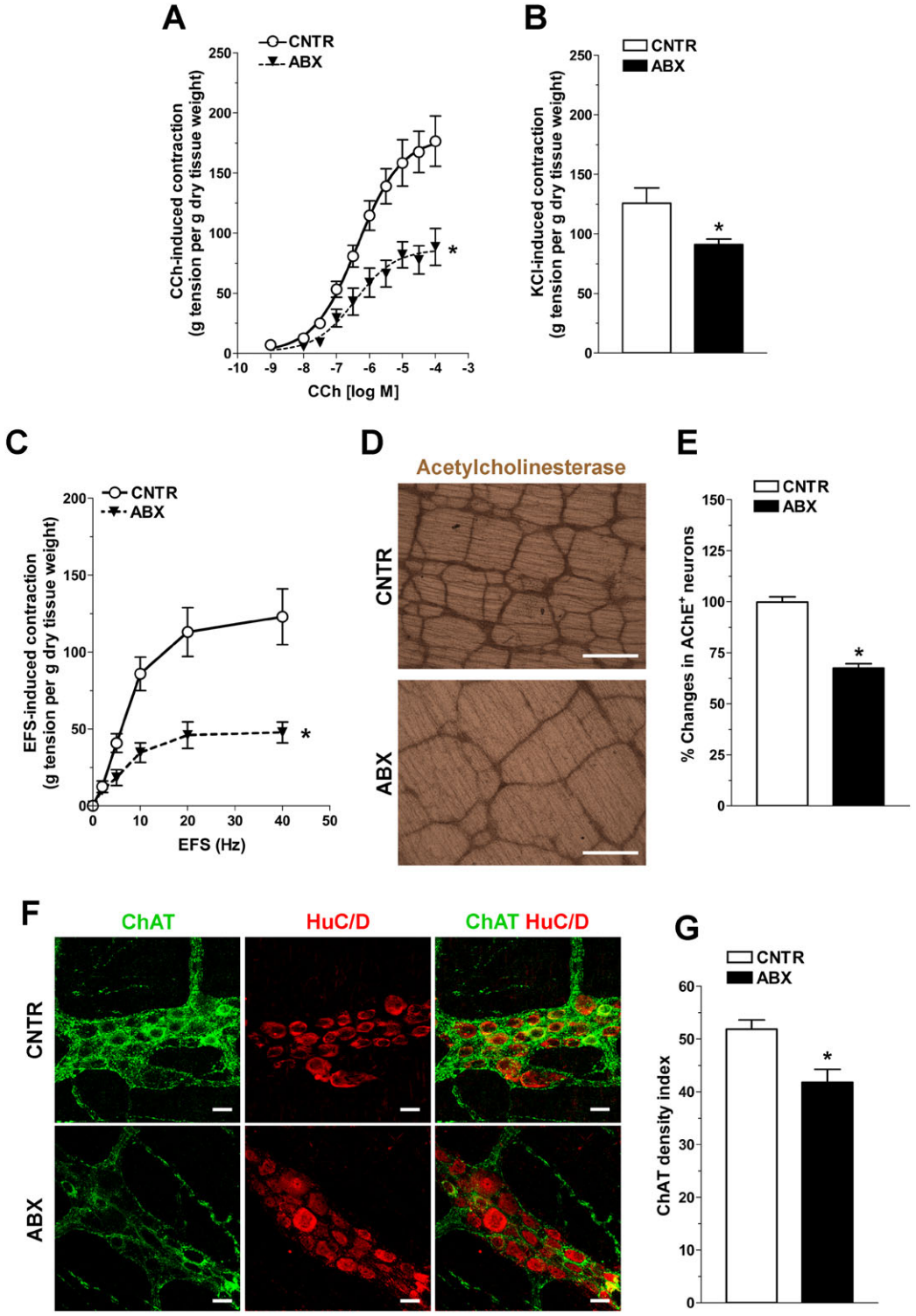

Figure 3

Antibiotic-induced dysbiosis influences excitatory contractility. (A) Concentration–response curves to carbachol (CCh) and (B) KCl 60 mM-elicited excitatory response in isolated ileal segments from CNTR and ABX-treated mice ($N = 16$ mice per group). (C) Neuromuscular excitatory response induced by EFS (0–40 Hz) in isolated ileal preparations of CNTR and ABX-treated mice ($N = 8$ mice per group). (D) Representative photomicrographs showing the distribution of $AChE^+$ neurons and (E) number of $AChE^+$ neurons per myenteric ganglia area in LMMP preparations of CNTR and ABX-treated mice ($N = 6$ mice per group). Scale bars = 200 μm. (F) Representative confocal photomicrographs showing the distribution of ChAT (green, marker for cholinergic neurons) and HuC/D (red, pan-neuronal marker) and (G) ChAT density index in LMMP preparations of CNTR and ABX-treated mice ($N = 6$ mice per group). Scale bars = 22 μm. Data are reported as mean ± SEM. *$P < 0.05$, significantly different from CNTR; one-way ANOVA followed by Newman–Keuls *post hoc* test (panels A and C) or unpaired Student's *t*-test (panels B, E and G).

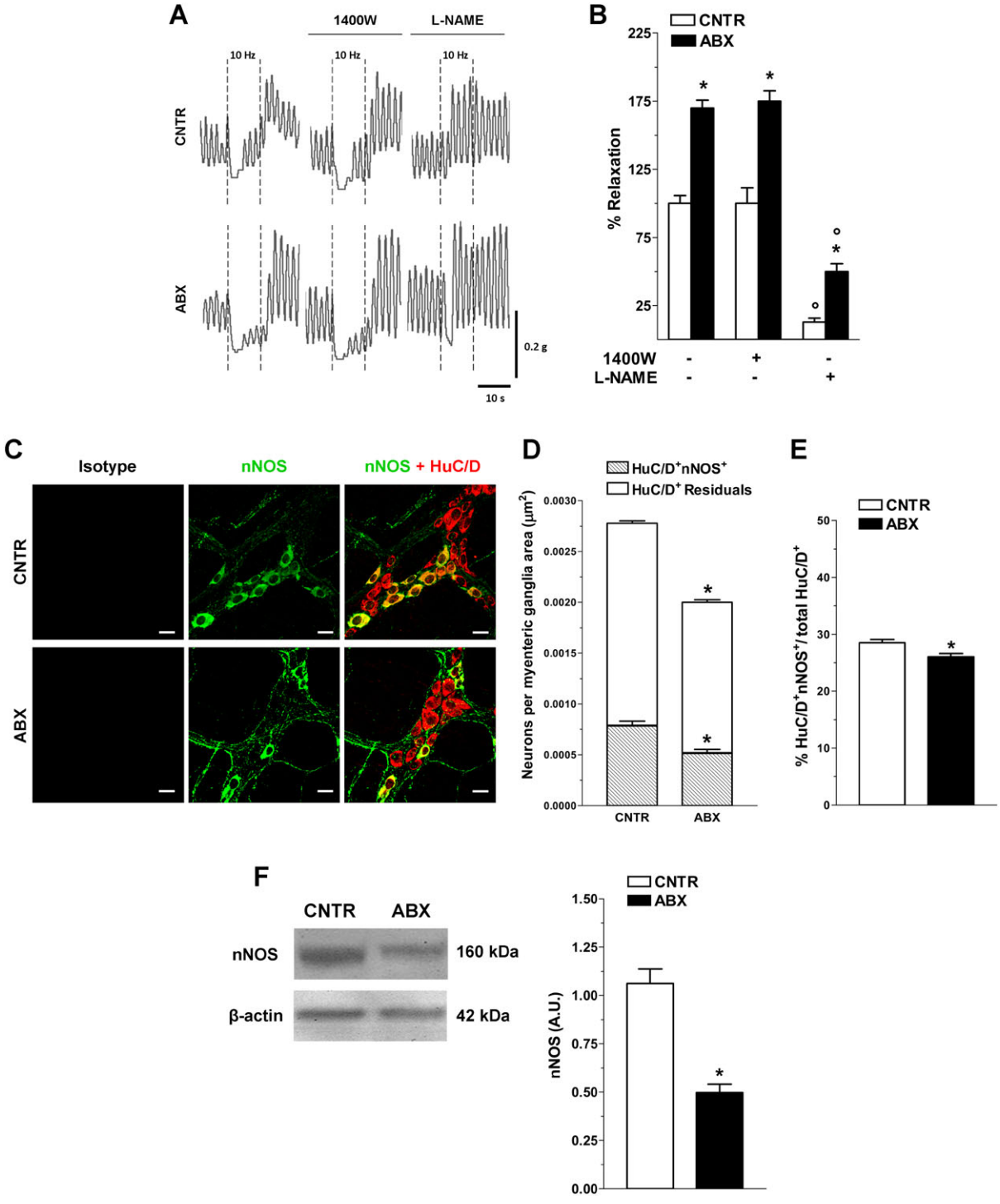

Figure 4

Antibiotic-induced microbiota dysbiosis affects inhibitory neurotransmission. (A) Representative tracings of on-relaxation responses induced by EFS at 10 Hz in ABX and CNTR segments under NANC conditions in absence or presence of 1400 W or L-NAME. (B) 10 Hz EFS-evoked NANC on-relaxation responses in absence or presence of 1400 W or L-NAME (N = 8 mice per group). (C) Representative confocal photomicrographs showing the distribution of nNOS (green; marker for nitrergic neurons) and HuC/D (red); (D) number of HuC/D$^+$nNOS$^+$ and residual HuC/D$^+$ neurons per myenteric ganglia area; (E) percentage of HuC/D$^+$nNOS$^+$ neurons respect to total HuC/D$^+$ neurons in ileal LMMP whole-mount preparations of CNTR and ABX-treated mice (N = 6 mice per group). Scale bars = 22 μm. (F) Western blot analysis of nNOS in protein extracts from ileal segments from ABX and CNTR mice (N = 6 per group). β-actin was used as loading control. Protein signals were quantified using densitometry analysis. Data are reported as mean ± SEM. *$P < 0.05$, significantly different from CNTR; °$P < 0.05$, significantly different from respective control without L-NAME; one-way ANOVA followed by Newman–Keuls *post hoc* test (panel A), paired or unpaired Student's *t*-test (panel B) or or unpaired Student's *t*-test (panels D, E and F).

neurons in the myenteric plexus. The number of nNOS$^+$ myenteric neurons was significantly reduced in the ileum of ABX-treated mice, compared with CNTR mice (N = 6 mice per group; Figure 4C–E). These changes were confirmed by the reduced nNOS protein levels in ileal samples from ABX-treated mice (N = 6 mice per group; Figure 4F), suggesting the involvement of other NANC transmitters, such as vasoactive intestinal peptide or ATP, in providing the increased ileal relaxation, in spite of the reduction of nNOS$^+$ neurons (Caputi *et al.,* 2017).

Substance P neurotransmission sustains ileum smooth muscle contractility following antibiotic-induced microbiota dysbiosis

To assess the contribution of other non-cholinergic excitatory neurotransmitters to neuromuscular function, we evaluated post-stimulus excitatory off-responses under NANC conditions in the presence of L-NAME, to unmask tachykininergic nerve-evoked contractions (Lecci *et al.,* 2006). The tachykinin-mediated response was increased in ABX-treated mice (N = 5 mice per group; Figure 5A) and this off-response was significantly reduced after selective blockade of NK_1 receptors with L732138 (Figure 5A).

In parallel, immunostaining for SP, a member of the tachykinin family of neuropeptides, with higher affinity for NK_1 than for NK_2 or NK_3 receptors (Lecci *et al.,* 2006), increased about 1.9-fold in the muscularis externa of ileal frozen sections of ABX-treated mice, relative to preparations obtained from CNTR animals (N = 5 mice per group; Figure 5B, C). A proportional significant increase of SP$^+$ neurons was observed in ileal myenteric plexus of ABX-treated mice (N = 5 mice per group; Figure 5D–F).

Functional involvement of TLR2 in ABX-treated juvenile mice

Because the interaction between gut microbiota and the host is mediated through TLRs, which are expressed throughout the whole intestine (Brun *et al.,* 2015), we evaluated TLR2 immunofluorescence in ileal frozen sections and whole-mount preparations. Antibiotic treatment increased TLR2 immunoreactivity in myenteric ganglia of LMMP whole-mount preparations (N = 5 mice per group, Figure 6A, B) and in neuromuscular and mucosal layers of ileal cryosections (N = 5 mice per group, Figure 6C, D). In ABX-treated mice, daily supplementation with the TLR2 agonist Pam3CSK4, given i.p., partly reversed the altered excitatory neuromuscular responses to carbachol (N = 8 mice per group; Figure 7A) and EFS (N = 8 mice per group; Figure 7B), suggesting that the gut microbial- and/or host-derived factors are involved in maintaining ENS homeostasis (Brun *et al.,* 2013).

Discussion

The symbiotic microbiota of the mammalian gut plays a key role in the development and preservation of bowel neuromotor activity by promoting several crucial functions, including pathogen defence, nutrition and maturation of the enteric nervous and immune systems (Hansen *et al.,* 2015). We here show, for the first time, the consequences of microbiota dysbiosis on the structure and function of juvenile ENS and provide novel insights into the affected pathways. In particular, this study demonstrates that microbiota dysbiosis during early adulthood has the following outcomes: (i) slowing of GI transit; (ii) altered morphology of the enteric glial bundles as well as changes in cholinergic, nitrergic and tachykinergic neurochemical coding; (iii) dysmotility of the small intestine associated with impaired cholinergic and nitrergic neurotransmission, increased SP-mediated motor response *via* NK_1 receptors; and (iv) increased TLR2 immunofluorescence intensity in the neuromuscular layers. To confirm the microbiota-mediated effect on ENS development, we activated, pharmacologically, the TLR2 pathway and found that defects in excitatory motor responses were partly corrected by treatment with the TLR2-specific agonist Pam3CSK4.

A two week course of high-dose antibiotics is a cost-effective model to assess the effects of gut dysbiosis on ENS integrity (Ubeda and Pamer, 2012). In our model, as in a germ-free phenotype, only the caecum and spleen showed macroscopic abnormalities. In addition, consistent with previous observations obtained after alteration of microbiota composition, gastric emptying and intestinal transit decreased, while the thickness of the muscularis externa in stomach, ileum and caecum increased, in ABX-treated mice (Barbara *et al.,* 2005; Reikvam *et al.,* 2011; Grasa *et al.,* 2015). Increased luminal levels of TCA were paralleled by the disappearance of CA in detectable levels, in ABX-treated mice. These findings were consistent with data from ampicillin-treated and germ-free mice (Sayin *et al.,* 2013) and confirmed the regulatory role of healthy gut microbiota in primary bile acid metabolism in the intestines. In agreement with other studies carried out in adult animals (Barbara *et al.,* 2005; Reikvam *et al.,* 2011; Brun *et al.,* 2013; Theriot *et al.,* 2016), these observations emphasize that commensal stimulation plays a key role for juvenile gut homeostasis, including regulation of the motor function of the intestine. In mammals, young adulthood represents a critical and dynamic phase for differentiation and maturation of neural circuits in the gut (Collins *et al.,* 2014). Several developmental changes occur postnatally, in the ENS. Although maturation of neural and glial cells within enteric mammalian ganglia takes place within the first 2 weeks of life, the on-going adaptive integration of neuron–glia units into the three-dimensional complex architecture continues for several weeks after birth (Kabouridis *et al.,* 2015). In our study, microbiota dysbiosis after antibiotic treatment during early adulthood affected the assembly of enteric neural circuits, reducing the number of neurons in the myenteric plexus, in analogy with results obtained in germ-free mice, TLRs knockout mice or autoimmune disorders (i.e. TLRs overstimulation) (Okun *et al.,* 2009; Brun *et al.,* 2013; Collins *et al.,* 2014). In addition, distortion of GFAP$^+$ processes and S100β overexpression are highly indicative of myenteric glial network alterations, which may underlie gut gliopathy due to a disrupted host–bacteria crosstalk. Besides exerting a trophic and functional support to enteric neurons, EGCs have been identified as key cellular targets for intestinal microflora. However, in this latter regard, the molecular mechanisms by which luminal microbiota shapes the organization of enteric neuroglial networks and its potential implication in GI disorders remains to be elucidated (Turco *et al.,* 2014; Kabouridis *et al.,*

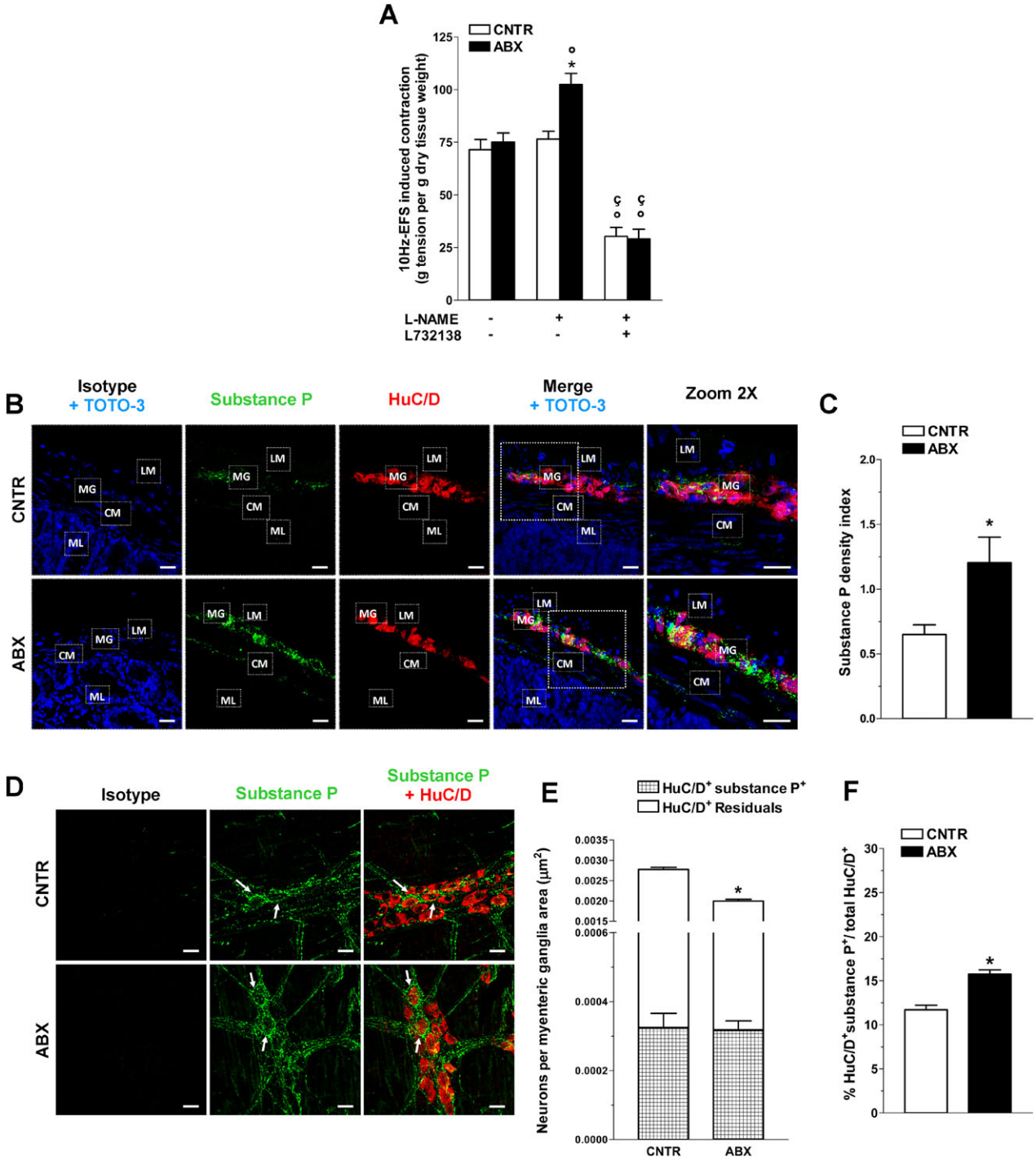

Figure 5

Antibiotic-induced microbiota dysbiosis increases SP-mediated response. (A) Tachykininergic-mediated response evoked by 10 Hz EFS in ileal preparations from CNTR and ABX-treated mice (N = 5 mice per group), under NANC conditions, in absence or presence of L-NAME or L732138. (B) Representative photomicrographs of frozen sections showing the distribution of SP (green) and HuC/D (red) and (C) SP density index in ileal neuromuscular layer from CNTR and ABX-treated mouse cryosections. Cell nuclei were stained with TOTO-3 (blue; N = 5 mice per group). Scale bars = 22 μm. (D) Representative microphotographs showing the distribution of SP (green) and HuC/D (red) and (E) number of HuC/D^+SP^+ and residual HuC/D^+ neurons per myenteric ganglia area and (F) percentage of SP^+ neurons respect to total HuC/D^+ neurons in ileal LMMP whole-mount preparations from CNTR and ABX mice (N = 5 mice per group). Scale bars = 22 μm. Arrows indicate SP^+HuC/D^+ neurons in myenteric plexus of CNTR and ABX mice. Data are reported as mean ± SEM. *$P < 0.05$, significantly different from CNTR; °$P < 0.05$, significantly different from respective control without L-NAME; '$P < 0.05$, significantly different from respective control without L732138; paired or unpaired Student's t-test (panel A) or unpaired Student's t-test (panels C, E and F). CM = circular muscle; LM = longitudinal muscle; MG = myenteric ganglia; ML = mucosal layer.

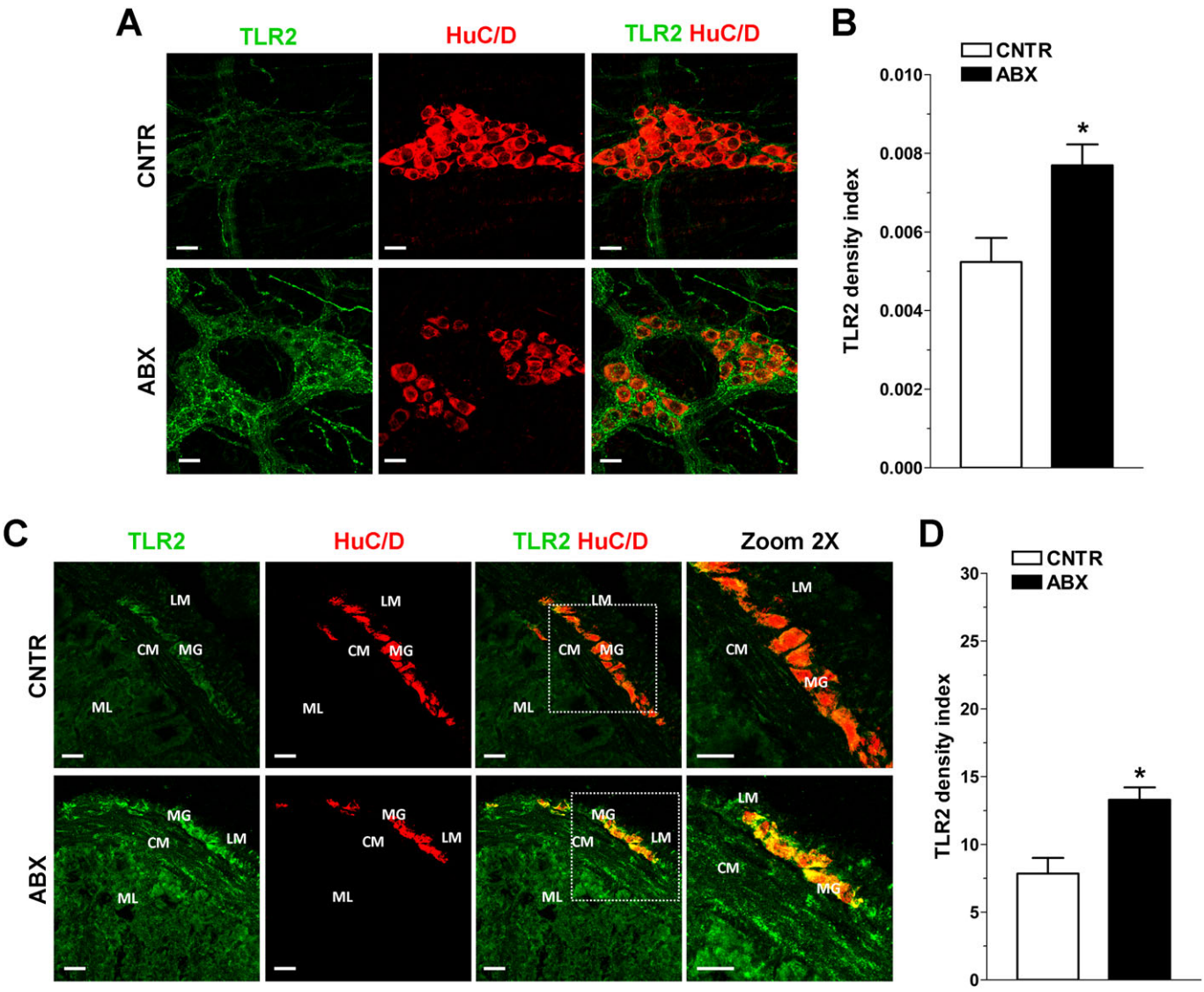

Figure 6

Antibiotic-induced microbiota dysbiosis influences ileal immunofluorescence distribution of TLR2. (A) Representative photomicrographs of the distribution of HuC/D (red) and TLR2 (green) and (B) TLR2 density index in LMMP whole-mount preparations from CNTR and ABX-treated mouse ileum (N = 5 mice per group). (C) Representative photomicrographs of the distribution of HuC/D (red) and TLR2 (green) and (D) TLR2 density index in ileal frozen sections from CNTR and ABX-treated mouse ileum (N = 5 mice per group). Scale bars = 22 μm. Data are reported as mean ± SEM. *$P < 0.05$, significantly different from CNTR; unpaired Student's t-test (panels B and D). CM = circular muscle; LM = longitudinal muscle; MG = myenteric ganglia; ML = mucosal layer.

2015). In ABX-treated mice, changes in ENS neurotransmitter pathways induced small bowel motor disturbances, resulting in a functional imbalance between excitatory and inhibitory neurotransmission. *In vitro* antibiotic treatment may alter gut neuromuscular contractility, either depressing the tone of isolated colonic muscularis mucosae, as with ampicillin, or potentiating cholinergic responses, as with vancomycin (Ceran *et al.*, 2006). However, our observations are in accordance with recently published studies suggesting that a dysbiosis, elicited *in vivo* by either antibiotic treatment or induced by either dietary changes or genetic deficiencies (i.e. TLRs deficiency), may either directly or indirectly affect gut motor and sensory function (Quigley, 2011; Brun *et al.*, 2013). In this respect, a reduction of $nNOS^+$ myenteric neurons together with an increased inhibitory neurotransmission, determined by the involvement of ATP pathways, has been observed in $TLR4^{-/-}$ mice, suggesting a key role of microbial-derived stimulation for ensuring gut homeostasis (Caputi *et al.*, 2017).

In the present study, we showed that antibiotic treatment increased SP immunoreactivity in the ileal neuromuscular compartment. SP is described as enteric neurotransmitter involved in the modulation of the enteric motor and sensory functions, and its intestinal content may be affected by bacteria perturbation or low-grade inflammation resulting from antibiotic treatment (Verdú *et al.*, 2006). Detection of

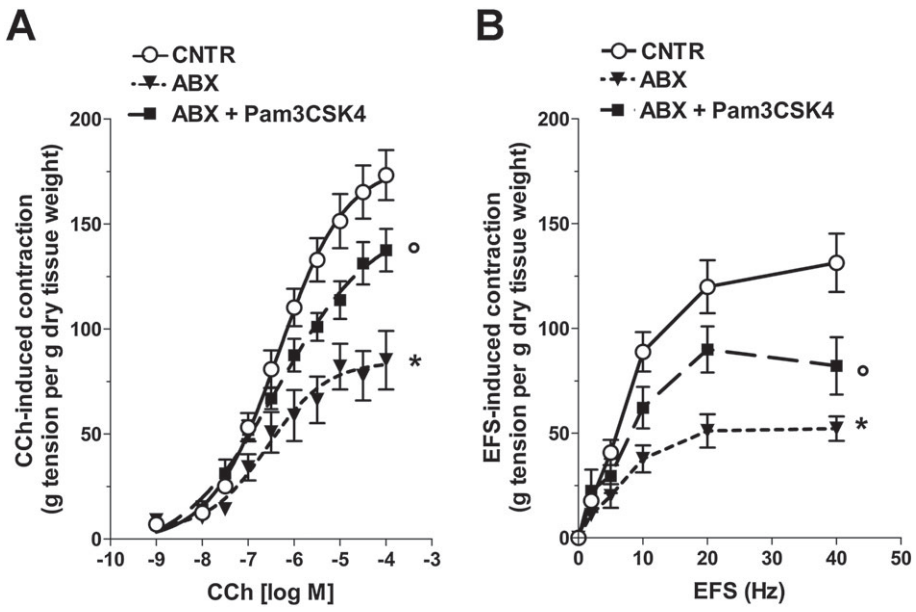

Figure 7

Pam3CSK4 administration improves excitatory neuromuscular contractility in ABX-treated mice. Concentration–response curves to (A) carbachol (CCh) and EFS-induced contractions (B) in isolated ileal preparations from CNTR, ABX-treated mice and ABX-treated mice after daily administration of Pam3CSK4 (N = 8 mice per group). Data are reported as mean ± SEM. *$P < 0.05$, significantly different from CNTR; °$P < 0.05$, significantly different from ABX-treated mice; two-way ANOVA followed by Bonferroni's *post hoc* test (panels A and B).

commensal bacteria by TLRs seems to represent an essential step to maintain the structural and functional integrity of ENS. Indeed, an impaired crosstalk between enteric commensals and TLRs may promote neurogliopathy, as observed in IBS and IBD (Frosali *et al.,* 2015; Barbara *et al.,* 2016). Gut dysbiosis enhanced immunofluorescence TLR2 signal both in neuromuscular and mucosal layers, suggesting the occurrence of a disrupted host–microbe interaction. The findings obtained in the present study, involving antibiotic-induced changes in TLR2 expression, nitrergic and tachykinergic enteric transmitter pathways, are consistent with those obtained in a recent study evaluating the influence of TLR2 signalling on ENS morphology and function (Brun *et al.,* 2013). In particular, up-regulation of TLR2 and SP pathways is all the more interesting because, in addition to its role in neurotransmission, SP can exert immunomodulatory activity and amplify innate immune responses by up-regulating TLR2 signalling (Tancowny *et al.,* 2010). The ability of a selective TLR2 agonist to restore excitatory motor responses after antibiotic treatment suggests that TLR2 stimulation by microbial- or/and host-derived factors can directly affect gut neuromuscular function. Consequently, we may infer from our data that an antibiotic therapy may reduce the availability of molecules, such as bacteria-derived lipopeptides, which *via* TLR2 activation retain a fundamental role in maintaining correct intestinal motor responses.

With the identification of the microbiota-gut-brain axis, it is tempting to propose that the morpho-functional defects observed in the ENS may set the basis for the phenotypic characteristics observed in a variety of diseases, ranging from depression and anxiety to IBS, obesity and neurodevelopmental disorders (Foster and McVey Neufeld, 2013; Crawford *et al.,* 2015; Barbara *et al.,* 2016; Bertrand *et al.,* 2016; Milleit *et al.,* 2016). Detrimental effects may thus affect the microbiota-host dialogue after antibiotic-induced dysbiosis, as, by perturbing the maturation of commensal microbiota composition as well as ENS development, the risk of developing chronic diseases (e.g. Crohn's disease) could be potentially much higher, as reported in observational studies in children (Ungaro *et al.,* 2014). Although our findings suggest that alterations of intestinal microflora may exert harmful effects on ENS development, we also provide evidence that activation of TLRs signalling by specific natural or synthetic agonists or by probiotics may have beneficial effect by restoring ENS integrity.

In conclusion, our study showed that perturbations of microbiota composition and consequent dysregulated host-bacteria interaction during early adulthood were critical as they significantly hampered ENS maturation and potentially established a phenotype susceptible to IBS and/or IBD (Brun *et al.,* 2013; Ungaro *et al.,* 2014; Barbara *et al.,* 2016). In addition, our findings also suggested that a 2 week high-dose course of antibiotics in juvenile mice represents a practical model for evaluating the effect of gut commensal bacteria on the maturation of juvenile ENS, without affecting the original postnatal gut microbiota composition, which is inevitable in germ-free mice. Finally, due to the emerging role of microbiota on gut activity and organization, and its potential relevance on gut functional disorders, further studies are needed to fully disclose the modulatory role of gut microbiota-derived factors on specific neurotransmission pathways and related effects on motility and pain perception, which may possibly predispose to gut disorders or preserve ENS developmental integrity.

Acknowledgements

We thank Dr. Francesca Patrese and Dr. Ludovico Scenna for veterinary assistance, Mauro Berto and Massimo Rizza for technical assistance in animal handling and experimental procedures and Vincenza Guzzardo for histological experiments. This work was supported by grants from University of Padova (UNIPD-Assegno di Ricerca 2016 and UNIPD-ex 60%-2015 and 2016 funds to M.C.G.) and from San Camillo Hospital, Treviso (Italy). The funders had no role in study design, data collection and analysis, decision to publish or preparation of the manuscript.

Author contributions

M.C.G., C.G., G.O., V.C. and P.D. conceived and designed the experiments. V.C., I.M., V.F., S.C., N.P., I.M.D.G., M.M., S.D.A., F.G. and M.B. performed the experiments. V.C., I.M., V.F., M.B., S.C., G.O., N.P., S.D.M., F.G., M.R., F.C., I.M.D.G., S.B., I.L., C.G. and M.C.G. analysed the data. M.C.G., C.G., I.L., S.B., F.C., M.M., S.D.M., S.D.A. and P.D. contributed reagents/materials/analysis tools. M.C.G., V.C., I.M., S.C., C.G., V.F., P.D., S.B. and I.M.D.G. wrote the manuscript. All the authors reviewed the manuscript.

Conflict of interest

The authors declare that the research was conducted in the absence of any commercial or financial relationships that could be construed as a potential conflict of interest.

Declaration of transparency and scientific rigour

This Declaration acknowledges that this paper adheres to the principles for transparent reporting and scientific rigour of preclinical research recommended by funding agencies, publishers and other organisations engaged with supporting research.

References

Alexander SPH, Fabbro D, Kelly E, Marrion N, Peters JA, Benson HE *et al*. (2015a). The Concise Guide to PHARMACOLOGY 2015/16: Catalytic receptors. Br J Pharmacol 172: 5979–6023.

Alexander SPH, Fabbro D, Kelly E, Marrion N, Peters JA, Benson HE *et al*. (2015b). The Concise Guide to PHARMACOLOGY 2015/16: Enzymes. Br J Pharmacol 172: 6024–6109.

Alexander SPH, Davenport AP, Kelly E, Marrion N, Peters JA, Benson HE *et al*. (2015c). The Concise Guide to PHARMACOLOGY 2015/16: G protein-coupled receptors. Br J Pharmacol 172: 5744–5869.

Anitha M, Vijay-Kumar M, Sitaraman SV, Gewirtz AT, Srinivasan S (2012). Gut microbial products regulate murine gastrointestinal motility via Toll-like receptor 4 signaling. Gastroenterology 143: 1006–16.e4.

Antonioli L, Giron MC, Colucci R, Pellegrini C, Sacco D, Caputi V *et al*. (2014b). Involvement of the P2X7 purinergic receptor in colonic motor dysfunction associated with bowel inflammation in rats. PLoS One 9 e116253.

Antonioli L, Fornai M, Awwad O, Giustarini G, Pellegrini C, Tuccori M *et al*. (2014a). Role of the A(2B) receptor-adenosine deaminase complex in colonic dysmotility associated with bowel inflammation in rats. Br J Pharmacol 171: 1314–1329.

Barbara G, Feinle-Bisset C, Ghoshal UC, Quigley EM, Santos J, Vanner S *et al*. (2016). The intestinal microenvironment and functional gastrointestinal disorders. Gastroenterology 150: 1305–1318.e8.

Barbara G, Stanghellini V, Brandi G, Cremon C, Di Nardo G, De Giorgio R *et al*. (2005). Interactions between commensal bacteria and gut sensorimotor function in health and disease. Am J Gastroenterol 100: 2560–2568.

Bertrand PP, Polglaze KE, Chen H, Sandow SL, Walduck A, Jenkins TA *et al*. (2016). Excitability and synaptic transmission in the enteric nervous system: does diet play a role? Adv Exp Med Biol 891: 201–211.

Borre YE, O'Keeffe GW, Clarke G, Stanton C, Dinan TG, Cryan JF (2014). Microbiota and neurodevelopmental windows: implications for brain disorders. Trends Mol Med 20: 509–518.

Brun P, Giron MC, Qesari M, Porzionato A, Caputi V, Zoppellaro C *et al*. (2013). Toll-like receptor 2 regulates intestinal inflammation by controlling integrity of the enteric nervous system. Gastroenterology 145: 1323–1333.

Brun P, Gobbo S, Caputi V, Spagnol L, Schirato G, Pasqualin M *et al*. (2015). Toll-like receptor-2 regulates production of glial-derived neurotrophic factors in murine intestinal smooth muscle cells. Mol Cell Neurosci 68: 24–35.

Caputi V, Marsilio I, Cerantola S, Roozfarakh M, Lante I, Galuppini F *et al*. (2017). Toll-like receptor 4 modulates small intestine neuromuscular function through nitrergic and purinergic pathways. Front Pharmacol 8: 350. https://doi.org/10.3389/fphar.2017.00350.

Ceran C, Karadas B, Kaya T, Arpacik M, Bagcivan I, Sarac B (2006). Do antibiotics contribute to postoperative ileus? Contractile responses of ileum smooth muscle in Guinea pigs to long-term parenteral ceftriaxone and ampicillin. ANZ J Surg 76: 1023–1026.

Coelho-Aguiar JM, Bon-Frauches AC, Gomes ALT, Veríssimo CP, Aguiar DP, Matias D *et al*. (2015). The enteric glia: identity and functions. Glia 63: 921–935.

Collins J, Borojevic R, Verdu EF, Huizinga JD, Ratcliffe EM (2014). Intestinal microbiota influence the early postnatal development of the enteric nervous system. Neurogastroenterol Motil 26: 98–107.

Crawford JD, Chandley MJ, Szebeni K, Szebeni A, Waters B, Ordway GA (2015). Elevated GFAP protein in anterior cingulate cortical white matter in males with autism spectrum disorder. Autism Res 8: 649–657.

Currò D, De Marco T, Preziosi P (2002). Involvement of peptide histidine isoleucine in non-adrenergic non-cholinergic relaxation of the rat gastric fundus induced by high-frequency neuronal firing. Naunyn Schmiedebergs Arch Pharmacol 366: 578–586.

Curtis MJ, Bond RA, Spina D, Ahluwalia A, Alexander SPA, Giembycz MA *et al*. (2015). Experimental design and analysis and their reporting: new guidance for publication in BJP. Br J Pharmacol 172: 3461–3471.

Dall'Olmo L, Fassan M, Dassie E, Scarpa M, Realdon S, Cavallin F *et al*. (2014). Role of proton pump inhibitor on esophageal carcinogenesis and pancreatic acinar cell metaplasia development: an experimental in vivo study. PLoS One 9 e112862.

Filpa V, Carpanese E, Marchet S, Pirrone C, Conti A, Rainero A *et al*. (2017). Nitric oxide regulates homeoprotein OTX1 and OTX2 expression in the rat myenteric plexus after intestinal ischemia-reperfusion injury. Am J Physiol Gastrointest Liver Physiol 312: G374–G389.

Foster JA, McVey Neufeld K-A (2013). Gut-brain axis: how the microbiome influences anxiety and depression. Trends Neurosci 36: 305–312.

Fröhlich EE, Farzi A, Mayerhofer R, Reichmann F, Jačan A, Wagner B *et al*. (2016). Cognitive impairment by antibiotic-induced gut dysbiosis: analysis of gut microbiota-brain communication. Brain Behav Immun 56: 140–155.

Frosali S, Pagliari D, Gambassi G, Landolfi R, Pandolfi F, Cianci R (2015). How the intricate interaction among Toll-like receptors, microbiota, and intestinal immunity can influence gastrointestinal pathology. J Immunol Res 2015: 489821.

Furness JB (2012). The enteric nervous system and neurogastroenterology. Nat Rev Gastroenterol Hepatol 9: 286–294.

Ge X, Ding C, Zhao W, Xu L, Tian H, Gong J *et al*. (2017). Antibiotics-induced depletion of mice microbiota induces changes in host serotonin biosynthesis and intestinal motility. J Transl Med 15: 13.

Giron MC, Bin A, Brun P, Etteri S, Bolego C, Florio C *et al*. (2008). Cyclic AMP in rat ileum: evidence for the presence of an extracellular cyclic AMP-adenosine pathway. Gastroenterology 134: 1116–1126.

Grasa L, Abecia L, Forcén R, Castro M, de Jalón JA, Latorre E *et al*. (2015). Antibiotic-induced depletion of murine microbiota induces mild inflammation and changes in toll-like receptor patterns and intestinal motility. Microb Ecol 70: 835–848.

Josefsdottir KS, Baldridge MT, Kadmon CS, King KY (2017). Antibiotics impair murine hematopoiesis by depleting the intestinal microbiota. Blood 129: 729–739.

Hansen TH, Gøbel RJ, Hansen T, Pedersen O (2015). The gut microbiome in cardio-metabolic health. Genome Med 7: 33.

Hyland NP, Cryan JF (2016). Microbe-host interactions: influence of the gut microbiota on the enteric nervous system. Dev Biol 417: 182–187.

Kabouridis PS, Lasrado R, McCallum S, Chng SH, Snippert HJ, Clevers H *et al*. (2015). The gut microbiota keeps enteric glial cells on the move; prospective roles of the gut epithelium and immune system. Gut Microbes 6: 398–403.

Kabouridis PS, Pachnis V (2015). Emerging roles of gut microbiota and the immune system in the development of the enteric nervous system. J Clin Invest 125: 956–964.

Kennedy PJ, Cryan JF, Dinan TG, Clarke G (2014). Irritable bowel syndrome: a microbiome-gut-brain axis disorder? World J Gastroenterol 20: 14105–14125.

Kilkenny C, Browne W, Cuthill IC, Emerson M, Altman DG (2010). Animal research: reporting *in vivo* experiments: the ARRIVE guidelines. Br J Pharmacol 160: 1577–1579.

Kuribayashi H, Miyata M, Yamakawa H, Yoshinari K, Yamazoe Y (2012). Enterobacteria-mediated deconjugation of taurocholic acid enhances ileal farnesoid X receptor signaling. Eur J Pharmacol 697: 132–138.

Lecci A, Capriati A, Altamura M, Maggi CA (2006). Tachykinins and tachykinin receptors in the gut, with special reference to NK2 receptors in human. Auton Neurosci 126–127: 232–249.

Li ZS, Schmauss C, Cuenca A, Ratcliffe E, Gershon MD (2006). Physiological modulation of intestinal motility by enteric dopaminergic neurons and the D2 receptor: analysis of dopamine receptor expression, location, development, and function in wild-type and knock-out mice. J Neurosci 26: 2798–2807.

Mayer EA, Knight R, Mazmanian SK, Cryan JF, Tillisch K (2014). Gut microbes and the brain: paradigm shift in neuroscience. J Neurosci 34: 15490–15496.

McGrath JC, Lilley E (2015). Implementing guidelines on reporting research using animals (ARRIVE etc.): new requirements for publication in BJP. Br J Pharmacol 172: 3189–3193.

McQuade RM, Carbone SE, Stojanovska V, Rahman A, Gwynne RM, Robinson AM *et al*. (2016). Role of oxidative stress in oxaliplatin-induced enteric neuropathy and colonic dysmotility in mice. Br J Pharmacol 173: 3502–3521.

Messenger JP, Furness JB (1990). Projections of chemically-specified neurons in the guinea-pig colon. Arch Histol Cytol 53: 467–495.

Milleit B, Smesny S, Rothermundt M, Preul C, Schroeter ML, von Eiff C *et al*. (2016). Serum S100B protein is specifically related to white matter changes in schizophrenia. Front Cell Neurosci 10: 33.

Okun E, Griffioen KJ, Lathia JD, Tang S-C, Mattson MP, Arumugam TV (2009). Toll-like receptors in neurodegeneration. Brain Res Rev 59: 278–292.

Quigley EMM (2011). Microflora modulation of motility. J Neurogastroenterol Motil 17: 140–147.

Reikvam DH, Erofeev A, Sandvik A, Grcic V, Jahnsen FL, Gaustad P *et al*. (2011). Depletion of murine intestinal microbiota: effects on gut mucosa and epithelial gene expression. PLoS One 6 e17996.

Robinson AM, Stojanovska V, Rahman AA, McQuade RM, Senior PV, Nurgali K (2016). Effects of oxaliplatin treatment on the enteric glial cells and neurons in the mouse ileum. J Histochem Cytochem 64: 530–545.

Sayin SI, Wahlström A, Felin J, Jäntti S, Marschall H-U, Bamberg K *et al*. (2013). Gut microbiota regulates bile acid metabolism by reducing the levels of tauro-beta-muricholic acid, a naturally occurring FXR antagonist. Cell Metab 17: 225–235.

Smith TK, Robertson WJ (1998). Synchronous movements of the longitudinal and circular muscle during peristalsis in the isolated guinea-pig distal colon. J Physiol 506: 563–577.

Sommer F, Bäckhed F (2013). The gut microbiota--masters of host development and physiology. Nat Rev Microbiol 11: 227–238.

Southan C, Sharman JL, Benson HE, Faccenda E, Pawson AJ, Alexander SPH *et al*. (2016). The IUPHAR/BPS guide to PHARMACOLOGY in 2016: towards curated quantitative interactions between 1300 protein targets and 6000 ligands. Nucl Acids Res 44: D1054–D1068.

Stenkamp-Strahm CM, Kappmeyer AJ, Schmalz JT, Gericke M, Balemba O (2013). High-fat diet ingestion correlates with neuropathy in the duodenum myenteric plexus of obese mice with symptoms of type 2 diabetes. Cell Tissue Res 354: 381–394.

Tancowny BP, Karpov V, Schleimer RP, Kulka M (2010). Substance P primes lipoteichoic acid- and Pam3CysSerLys4-mediated activation of human mast cells by up-regulating Toll-like receptor 2. Immunology 131: 220–230.

Theriot CM, Bowman AA, Young VB (2016). Antibiotic-induced alterations of the gut microbiota alter secondary bile acid production and allow for *Clostridium difficile* spore germination and outgrowth in the large intestine. mSphere 1 e00045-15.

Turco F, Sarnelli G, Cirillo C, Palumbo I, De Giorgi F, D'Alessandro A *et al*. (2014). Enteroglial-derived S100B protein integrates bacteria-induced Toll-like receptor signalling in human enteric glial cells. Gut 63: 105–115.

Ubeda C, Pamer EG (2012). Antibiotics, microbiota, and immune defense. Trends Immunol 33: 459–466.

Ungaro R, Bernstein CN, Gearry R, Hviid A, Kolho K-L, Kronman MP *et al*. (2014). Antibiotics associated with increased risk of new-onset Crohn's disease but not ulcerative colitis: a meta-analysis. Am J Gastroenterol 109: 1728–1738.

Verdú EF, Bercik P, Verma-Gandhu M, Huang X-X, Blennerhassett P, Jackson W *et al*. (2006). Specific probiotic therapy attenuates antibiotic induced visceral hypersensitivity in mice. Gut 55: 182–190.

Zizzo MG, Mule F, Serio R (2003). Duodenal contractile activity in dystrophic (mdx) mice: reduction of nitric oxide influence. Neurogastroenterol Motil 15: 559–565.

Zizzo MG, Mulè F, Serio R (2004). Interplay between PACAP and NO in mouse ileum. Neuropharmacology 46: 449–455.

Zoppellaro C, Bin A, Brun P, Banzato S, Macchi V, Castagliuolo I *et al*. (2013). Adenosine-mediated enteric neuromuscular function is affected during herpes simplex virus type 1 infection of rat enteric nervous system. PLoS One 8 e72648.

Supporting Information

Additional Supporting Information may be found online in the supporting information tab for this article.

https://doi.org/10.1111/bph.13965

Figure S1 Antibiotic-induced dysbiosis of microbiota produces a germ free-like phenotype. (A) Representative photographs of murine caecum-colon tract of CNTR and ABX-treated mice. (B and C) Changes in caecum and spleen weights in CNTR e ABX-treated mice (N = 5 mice per group). Data are reported as mean ± SEM. * $P < 0.05$, significantly different from CNTR; unpaired Student's *t* test.

Figure S2 Antibiotic-induced microbiota dysbiosis affects pellet frequency and faecal water content. (A) Total number of faecal pellets expelled from CNTR or ABX-treated mice in 1 h collection period (N = 15 mice per group). (B) Wet and dry weight of faecal pellets expelled from CNTR or ABX-treated mice. (C) Percentage of faecal water content of CNTR and ABX-treated mice (N = 15 mice per group). Data are reported as mean ± SEM. Statistical significance was determined using unpaired Student's *t* test. * $P < 0.05$, significantly different from CNTR.

Table S1 Primary and secondary antisera and their respective dilutions used for immunohistochemistry on ileal whole-mount preparations and frozen sections.